ADVANCED FUNCTIONAL MATERIALS
www.afm-journal.de

Stretchable Self-Powered Fiber-Based Strain Sensor

*Junwen Zhong, Qize Zhong, Qiyi Hu, Nan Wu, Wenbo Li, Bo Wang, Bin Hu, and Jun Zhou**

The rapid development of electrical skin and wearable electronics raises the requirement of stretchable strain sensors. In this study, an active fiber-based strain sensor (AFSS) is fabricated by coiling a fiber-based generator around a stretchable silicone fiber. The AFSS shows the sensitive and stable performance and has the ability to detect the strain up to 25%, which is also demonstrated to detect finger motion states. It may play an essential role in future self-powered sensor system.

1. Introduction

The rapid evolution of biotechnology and communication brings a wide spectrum of opportunities to change our surroundings into an intelligent world, where a group of smart sensing systems are prerequisite.[1] The market of sensing systems, especially in electrical skin (e-skin) and wearable electronics is foreseen to skyrocket in the coming year.[1–6] Those sensors could transduce the physiological stimuli including strain,[6–8] moisture[9] into electrical signals, with the applications in intelligent robotic systems,[7] while promising route towards the development of high-performance strain sensors requires a rational design and innovative device model.

In recent years, many stretchable strain sensors based on piezoresistive effect, such as insulating polymers with conductive additives as the active layer, were reported.[10,11] This kind of strain sensors even has the ability to detect strains up to 280%.[11] However, bias voltage was inevitable for these sensors during the operation, which would increase the device cost considering external power supply or battery usage. Alternatively, the strain sensors based on piezoelectric effect of ZnO[12–14] or other perovskite materials[15,16] can simplify the device unitizing their unique self-powered characterization. However, their mechanical properties limit the applications in stretchable field with the strain higher than 5%.[16] Besides, compared with conventional solid metal electrodes,[17–20] which usually retain a static shape once fabricated, a stretchable electrode that can withstand bend or twist is also urgently needed for stretchable sensors.[10,11] However, the development from flexible device to a stretchable device remains an elusive goal.

Here, we introduce an active fiber-based strain sensor (AFSS) utilizing electrostatic effect, which is made up of two kinds of pretreated cotton threads, one was carbon nanotube (CNT)-coated cotton threads (CCT), and the other was polytetrafluoroethylene (PTFE) and carbon nanotube-coated-cotton threads (PCCT), these two threads were entangled to form an double-helixes structure generator, and then the generator was coiled around a silicone fiber to form an AFSS. The AFSS showed sensitive and stable performance and could detect the strain up to 25% by virtue of the helix device structure and highly stretchable silicone fiber. Additional, we introduced a new sensing mechanism of the self-powered strain sensor by measuring the quantity of the transfer changes, which vary linearly with the changed stimulated strains, and are uninfluenced by the stimulated frequencies. Furthermore, our device was demonstrated to detect finger motion states. This study indicates that the AFSS has potential applications in future self-powered sensor system by detecting the mechanical deformation of the human body and surrounding environment.

2. Results and Discussion

The fabrication process of an AFSS is schematically shown in Figure S1 (Supporting Information). Specifically, the AFSS was fabricated by twinning two kinds of pretreated cotton threads, which were the CCT and the PCCT, to form a double-helixes structure generator (length of 11.7 cm), and then the generator was coiled around a stretchable silicone fiber to form a helix structure device (length of 9.1 cm, **Figure 1**a). The scanning electron microscopy (SEM) image of the CCT surface is shown in Figure 1b, indicating that the CCT surface was fully covered by conductive multiwall CNTs, which were interlaced together. The fabrication method and the physical performance of CCT, such as the conductivity and mechanical property, were reported in our previous work, as well as the fabrication method of PCCT.[21] Figure 1c shows the atomic force microscopy (AFM) image of the PCCT surface, it can be seen that the surface was rather rough and the PTFE layer was composed of oval-like PTFE nanoparticles with diameters below 200 nm. Simultaneously, the relative height of the surface was measured along the white line in Figure 1c and it varied from ≈40 to ≈–50 nm (Figure 1d). Ideally,

J. W. Zhong, Q. Z. Zhong, Q. Y. Hu, N. Wu, W. B. Li, B. Wang, Dr. B. Hu, Prof. J. Zhou
Wuhan National Laboratory for Optoelectronics and School of Optical and Electronic Information
Huazhong University of Science and Technology
Wuhan 430074, China
E-mail: jun.zhou@mail.hust.edu.cn
B. Wang
Department of Electrical Engineering and Automation
Luoyang Institute of Science and Technology
Luoyang 471023, China

DOI: 10.1002/adfm.201404087

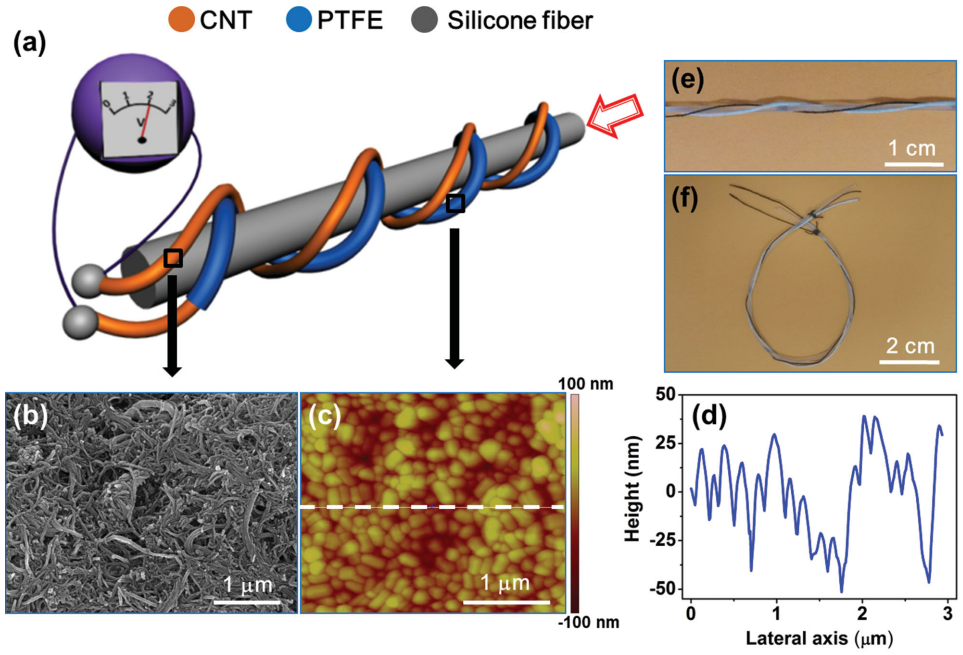

Figure 1. The structure and physical properties of an AFSS. a) Schematic diagram of an AFSS. b) SEM image of the surface of CCT and c) AFM image of the surface of PCCT. d) The relative altitude along the white line in (c). The digital photos of an AFSS with e) linear shape and f) curved shape.

the nanoscaled roughness can increase the specific surface area of PCCT, which is helpful to store more residual charges. The digital images of the AFSS are shown in Figure 1e,f, owing to the cushioning property of the helix device structure and the highly stretchable ability of the silicone fiber, the AFSS is high flexible and stretchable, ensuring its practical application.

To investigate the proposed working mechanism of the AFSS, the electric potential distribution and the charge transfer resulted from the air gap changing between the two fibers can be evaluated by a finite element simulation (COMSOL Multiphysics software). As discussed above, an AFSS is composed of CCT, PCCT, and silicone fiber. Due to the PTFE of PCCT can be considered as an electric field source,[22,23] obtaining the surface potential of PTFE is of great necessity, thus the change of surface potentials of PCCT versus time was investigated in **Figure 2**a. The surface potential decayed exponentially from –518 to – 254 V

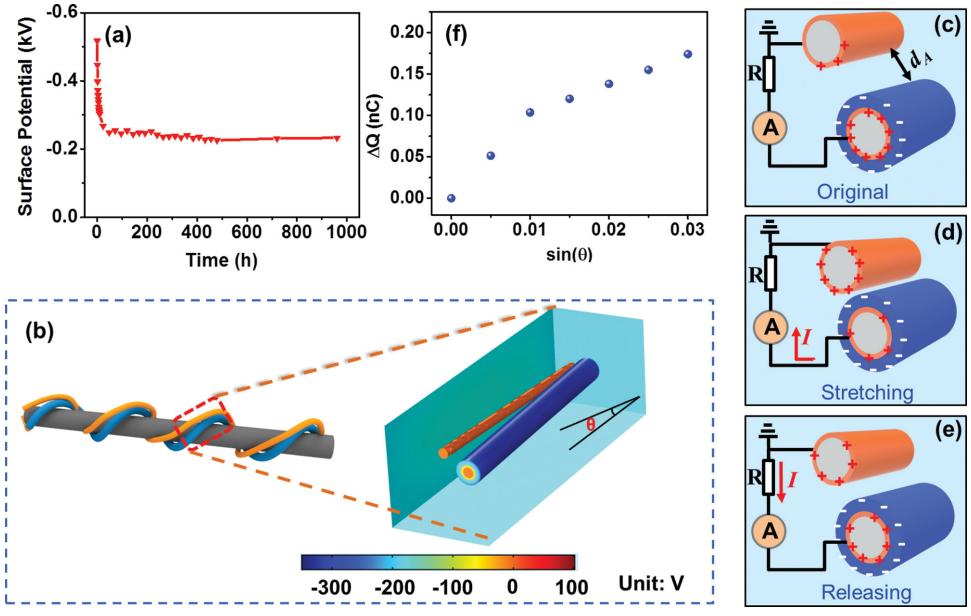

Figure 2. Working mechanism of an AFSS based on finite element simulation. a) Surface potential decay of the PCCT. b) The finite element simulation of the working mechanism for an AFSS. Schematic diagram illustrating the power generation mechanism of the AFSS with an external load of R when the device at c) original, d) stretching, and e) releasing states, respectively. f) The theoretical transferred charges according to the finite element simulation.

for 72 h, and then maintained in a narrow range for natural attenuation, the process of which was monitored by an electrostatic meter as shown in Figure S2 (Supporting Information).

Since the output performance was mainly depends on the air gap distance between CCT and PCCT during stretching and releasing for simplicity, COMSOL model ignored the silicone fiber, which has little effect on the results, and considering the symmetry of the coiling cycle unit in the AFSS device, only half a unit of a single coiling cycle is constructed for simulation. Initially, two fibers have an angle of θ (Figure 2b), and the potential change of the AFSS in a complete cycle when stretching and releasing are illustrated in Figure S3 (Supporting Information). Assume the charge distribution on the PTFE surface of PCCT fiber was uniform[21] because of its isolated property. Positive charges would be induced on two electrodes through electrostatic induction, as shown in Figure 2c. Figure S3a (Supporting Information) displays an original steady state of an AFSS. There was no electrical potential difference between two electrodes, shown in Figure S3a (Supporting Information) right view explicitly, meaning no electrons would occur in the interfacing circuit. Once the silicone fiber was stretched and the gap between the CCT and PCCT would decrease, the charges and potential on the constrained "double-helix" fibers would redistribute due to the decreased angle θ. As illustrated in Figure S3b (Supporting Information), the simulated result shows that the potential in PCCT was higher than that in CCT, which would drive the free electrons from CCT to PCCT through the external circuit to balance the potential difference (Figure 2d), and then another steady state could be achieved after stretching as shown in Figure S3c (Supporting Information). Once releasing, the gap between the CCT and PCCT and the angle of θ would increase, so the potential equilibrium was unbalanced again (Figure S3d, Supporting Information), and the electrons would flow back from the PCCT electrode with higher potential to CCT, to build a new equilibrium (Figure 2e). Specially, the charge transfer dependence of the $\sin(\theta)$ value in the model could be calculated using a charge quantity probe. As illustrated in Figure 2f, the graph reveals that our AFSS has the capability in acting as an active strain sensor.

The typical electrical output performance of the AFSS with length of 9.1 cm and 6 coiling turns was systematically studied by periodically stretching and releasing the AFSS with controlled frequencies and strains. The measuring system is schematically shown in Figure S4 (Supporting Information). One end of the AFSS was fixed on an x-y-z 3D mechanical stage, which was mounted tightly on an optical table, while another end was fixed on the resonator. The output currents through an external load of 40 MΩ were monitored all the time.

Obviously, the electrical output performances of the AFSS are affected by the coiling turns around the silicone fiber. It can be seen in Figure S5 (Supporting Information) that an AFSS with six coiling turns exhibited the highest load peak currents and integral transferred charges under 2.2% stimulated strain and 5 Hz frequency. It is clearly understood that the windings of the threads are dominated by the net length of the fiber-based sensors and the mechanics of structure, which would result in the distinction of gap changing. For our AFSS with a net length of 11.7 cm, either the loose state with four windings or tensed state with eight windings would result in smaller gap distance changing. Based on this fact, the AFSS with six coiling turns was selected.

Figure S6a (Supporting Information) shows the stimulated output currents of an AFSS varied with different strains at a given frequency of 5 Hz. Generally, the load peak currents increased linearly, from ≈1.05 nA at 0.55% to ≈5.20 nA at 2.75%, with the increased strains. The integral transferred charges curves corresponding to each positive current peak are shown in Figure S6b (Supporting Information), indicating that integral transferred charges changed linearly, from ≈0.048 nC at 0.55% to ≈0.147 nC at 2.75%, as well as the load peak currents variation tendency (**Figure 3**a). The above results clearly indicate that the integral transferred charges rely on the stimulated strains.

The output performance depended on the stretching/releasing frequency was also studied at a given strain of 2.5%. As the frequencies increased gradually, the stimulated load peak currents of the AFSS increased linearly from ≈0.95 nA at 1.3 Hz to ≈5.17 nA at 6 Hz as well, (Figure S6c, Supporting Information). Generally, the deformation between the CCT and PCCT kept constant for a given simulated strain and different simulated frequencies, so the integral transferred charges were theoretically the same according to our previous work.[22,23] Figure S6d (Supporting Information) and Figure 3b show the integral transferred charges of each positive current peak at different stimulated frequencies almost kept constant of ≈0.135 nC for different stimulated frequencies.

In conventional piezoelectric strain sensor, the output voltage/current of strain sensor are used to evaluate the magnitude of applied strains.[24–26] While according to above results, the output current varied with stimulated frequency increasing, indicating that the current/voltage data were unsuitable to evaluate our AFSS. However, the transferred charges varied linearly with the applied strains and were uninfluenced by the stimulated frequency, thus the AFSS can be utilized as a strain sensor by measuring the integral transferred charges.

On the other hand, the stability of the AFSS's output is a very essential factor to ensure its application as a reliable strain sensor. In our study, an AFSS was stretched and released continuously and repeatedly for 90 000 cycles at a stimulated strain of 2.2% and frequency of 5 Hz, and typical data of 1 min in each hour was shown in Figure 3c. It can be found that the load peak current of the device showed little variation during 5 h continuous working, and the integral transferred charges curves were almost the same as well (Figure 3c), only with a variation of −1.48% to 1.85% (Figure 3d). The SEM image in Figure S7 (Supporting Information) proved that no noticeably surface morphology degradation of PCCT and CCT was observed after test, and this high stability of the AFSS is benefited from the high flexibility of PCCT and CCT, and unique design of helical structure.

The effect of various environmental factors, including humidity and temperature, to the output of our AFSS has also been studied. It could be found that the temperature changing from ≈20 °C to ≈45 °C with a constant humidity (of ≈30% RH) has negligible effect on our fiber-based sensor, as shown in Figure S8 I and II (Supporting Information). In our study, the humidity has slight effect to the output current of our AFSS.

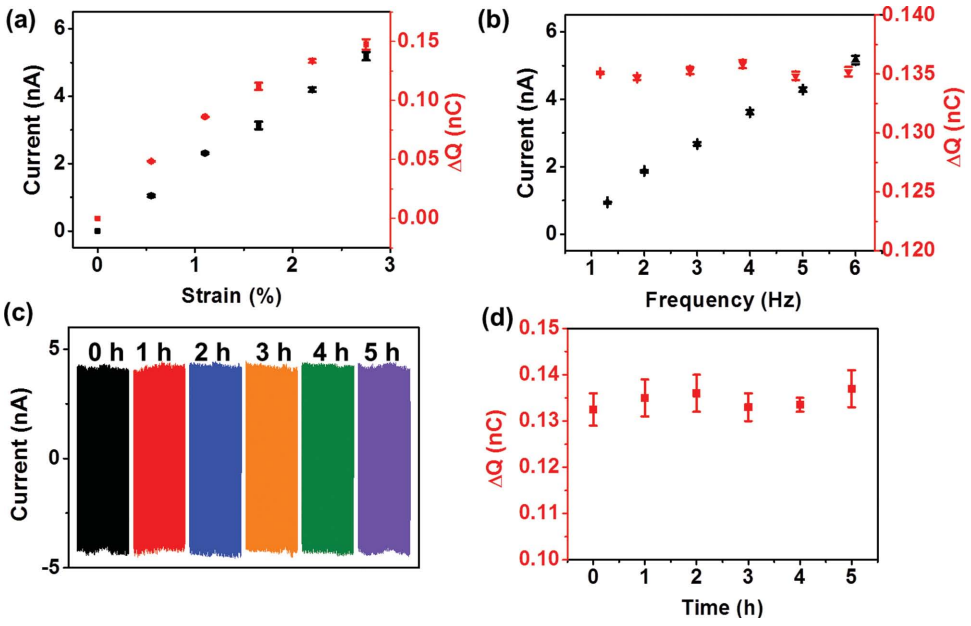

Figure 3. The electrical output performances of an AFSS through an external load of 40 MΩ under different testing conditions. The peak value of the output currents and integral transferred charges of an AFSS varied with a) stimulated strains of 0, 0.55%, 1.10%, 1.65%, and 2.75% for a given frequency of 5 Hz and b) stimulated frequencies of 1.3, 2, 3, 4, 5, and 6 Hz for a given strain of 2.20%. c) Typical 1 min output current data for 5 h (≈90 000 cycles) continuous stimulation of the AFSS and d) the variation of integral transferred charges over time.

As illustrated in Figure S8 I and III (Supporting Information), the output currents have only a 7.5% decline when the humidity rises up from ≈30% RH to ≈75% RH at a temperature of ≈20 °C.

The helix structure brings the excellent stretchability, which endows the AFSS the capability of detecting high degree strains. To demonstrate that, one end of the AFSS was fixed on a table; another end was pulled by hand to different degree of strains. In each motion state, the AFSS was pulled to the same degree of strain and then released for three cycles. During each pulling and releasing process, a couple of output current signals with opposite polarity would be generated (**Figure 4**a). As above results, the load peak currents are relative to both of motion speeds and motion amplitudes, but the integral transferred charges are only corresponding to the motion amplitudes. In our experiments, degree of strains from 5% to 25% was applied on an AFSS. The integral transferred charges curves corresponding to each positive current peak, as shown in Figure 4b,c, indicate that the integral transferred charges increased with the increasing of strain.

To demonstrate a specific application of the AFSS, it was fixed on a finger to detect the finger motion states (Video 1, Supporting Information). Specifically, the currents generated by the finger motions were rectified and the generating charges were stored in a 1 nF commercial capacitor, which would generate voltage across the capacitor. Then, a detector was utilized to detect the voltage and the results were shown on a screen (Figure 4d and Figure S9, Supporting Information). When the finger did not move at all, no signal was observed, as shown in Figure 4e. If the finger moved with a little amplitude, the detector would response, as shown in Figure 4f. Once the moving amplitude was larger enough, the sensor would be triggered, turning green to red on the screen, as shown in Figure 4g. This study indicated that the AFSS can be used as a self-powered active strain sensor for detecting human motion, and has potential application in personal health and environmental vibration detection.

3. Conclusion

In summary, a self-powered AFSS was fabricated by coiling a fiber-based generator, which was made by twining CCT and PCCT fibers together, around a stretchable silicone fiber. The AFSS can be utilized as a strain sensor by measuring the integral transferred charges and showed excellent sensitivity and stability. Simultaneously, up to 25% strain could be detected by the AFSS and it could be demonstrated to detect finger motion states. Furthermore, this work introduces a new sensing mechanism of self-power strain sensor by measuring the quantity of the transfer changes to evaluate the strains. This study extends the applications of fiber-based generators and proves that the AFSS may have applications in personal health monitor.

4. Experimental Section

Fabrication of an Active Fiber-Based Strain Sensor: The fabrication process of CCT and PCCT was reported by our previous work. In a detail fabrication process of an AFSS, a CCT and a PCCT were twined by each other to form a double-helixes structure device by adjusting the

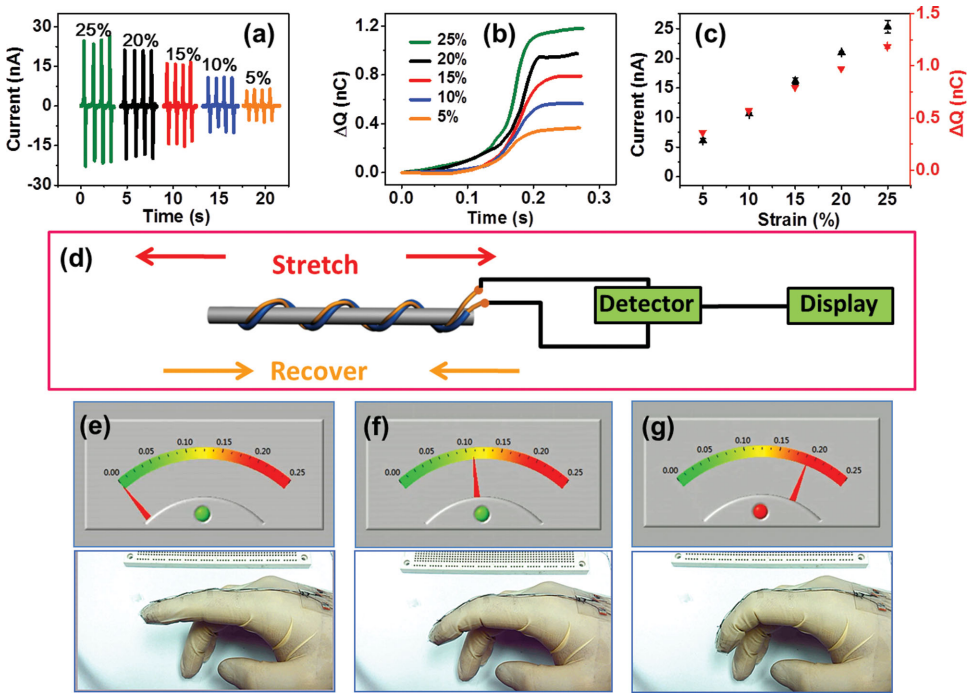

Figure 4. An AFSS for detecting high degree strains and body motion. a) Output current–time curves, b) corresponding integral transferred charges curves and c) the peak value of the output currents and integral transferred charges of an AFSS varied with stimulated strains of 5%, 10%, 15%, 20%, and 25%. d) The schematic diagram for detecting finger motion states. The detecting results and digital photos show the fingers e) did not move, f) moved with little amplitude, and g) large amplitude.

helix turns and leaving gaps and two ends of the device were fixed by commodity cotton threads. Then, the double-helixes structure device was surrounded around the stretchable silicone fiber by adjusting the coiling turns and its two ends were fixed by commodity cotton threads too.

Characterization: The morphology of samples was probed by a high-resolution field emission scanning electron microscope (FEI Nova Nano SEM 450) and AFM. The surface potential of PTFE was detected by an electrometer (EST102, Huajing Beijing, China). Periodically, stretching–releasing process of the AFSS was stimulated periodically by a resonator (JZK, Sinocera, China), which was controlled by a swept signal generator (YE 1311-D, Sinocera, China). The performance measurement system of the AFSS is schematically shown in Figure S3 (Supporting Information), which one end of the AFSS was fixed on an x-y-z mechanical stage mounted tightly on an optical table, while another end fixed on the resonator. During the measurement process, AFSS was periodically stretched and released with different degree of strain and frequency by the resonator (JZK, Sinocera, China). Simultaneously, the current signals through an external load of 40 MΩ were measured by a Stanford low-noise current preamplifier (Model SR570).

Supporting Information

Supporting Information is available from the Wiley Online Library or from the author.

Acknowledgements

J.W.Z. and Q.Z.Z contributed equally to this work. This work was financially supported by the National Natural Science Foundation of China (51322210, 61434001), a Foundation for the Author of National Excellent Doctoral Dissertation of PR China (201035) and Director Fund of WNLO. The authors thank to the facility support of the Center for Nanoscale Characterization & Devices, WNLO-HUST, and the Analysis and Testing Center of Huazhong University of Science and Technology.

Received: November 18, 2014
Revised: January 8, 2015
Published online: February 4, 2015

[1] D. Kim, N. Lu, R. Ma, Y. S. Kim, R. Kim, S. Wang, J. Wu, S. Won, H. Tao, A. Islam, K. Yu, T. Kim, R. Chowdhury, M. Ying, L. Xu, M. Li, H. Chung, H. Keum, M. McCormick, P. Liu, Y. Zhang, F. Omenetto, Y. Huang, T. Coleman, J. A. Rogers, *Science* **2011**, *333*, 838.
[2] L. Pan, A. Chortos, G. Yu, Y. Wang, S. Isaacson, R. Allen, Y. Shi, R. Dauskardt, Z. Bao, *Nat. Commun.* **2014**, *5*, 3002.
[3] S. Gong, W. Schwalb, Y. Wang, Y. Chen, Y. Tang, J. Si, B. Shirinzadeh, W. Cheng, *Nat. Commun.* **2013**, *5*, 3132.
[4] C. Wang, D. Hwang, Z. Yu, K. Takei, J. Park, T. Chen, B. Ma, A. Javey, *Nat. Mater.* **2013**, *12*, 899.
[5] X. Wang, Y. Gu, Z. Xiong, Z. Cui, T. Zhang, *Adv. Mater.* **2014**, *26*, 1336.
[6] G. Schwartz, B. C. K. Tee, J. Mei, A. L. Appleton, D. H. Kim, H. Wang, Z. Bao, *Nat. Commun.* **2013**, *4*, 1859.
[7] K. Takei, T. Takahashi, J. C. Ho, H. Ko, A. G. Gillies, P. W. Leu, R. S. Fearing, A. Javey, *Nat. Mater.* **2010**, *9*, 821.
[8] X. Xiao, L. Yuan, J. Zhong, T. Ding, Y. Liu, Z. Cai, Y. Rong, H. Han, J. Zhou, Z. L. Wang, *Adv. Mater.* **2011**, *23*, 5440.
[9] J. Feng, L. Peng, C. Wu, X. Sun, S. Hu, C. Lin, J. Dai, J. Yang, Y. Xie, *Adv. Mater.* **2012**, *24*, 1969.
[10] D. Lipomi, M. Vosgueritchian, B. Tee, S. Hellstrom, J. Lee, C. Fox, Z. Bao, *Nat. Nanotechnol.* **2011**, *6*, 788.

[11] T. Yamada, Y. Hayamizu, Y. Yamamoto, Y. Yomogida, A. Izadi-Najafabadi, D. Futaba, K. Hata, *Nat. Nanotechnol.* **2011**, *6*, 296.
[12] J. Zhou, Y. Gu, P. Fei, W. Mai, Y. Gao, R. Yang, G. Bao, Z. L. Wang, *Nano Lett.* **2008**, *8*, 3035.
[13] S. Lee, S. Bae, L. Lin, Y. Yang, C. Park, S. Kim, S. Cha, H. Kim, Y. Park, Z. L. Wang, *Adv. Funct. Mater.* **2013**, *23*, 2445.
[14] S. Lee, R. Hinchet, Y. Lee, Y. Yang, Z. Lin, G. Ardila, L. Montès, M. Mouis, Z. L. Wang, *Adv. Funct. Mater.* **2014**, *24*, 1163.
[15] J. Wu, C. Chen, Y. Zhang, K. Chen, Y. Yang, Y. Hu, J. He, Z. L. Wang, *ACS Nano* **2012**, *6*, 4369.
[16] J. Zhang, B. Xiang, Q. He, J. Seidel, R. Zeches, P. Yu, S. Yang, C. Wang, Y. Chu, L. Martin, A. Minor, R. Ramesh, *Nat. Nanotechnol.* **2011**, *6*, 98.
[17] F. Xu, Y. Zhu, *Adv. Mater.* **2012**, *24*, 5117.
[18] T. Trung, N. Tien, D. Kim, M. Jang, O. Yoon, N. Lee, *Adv. Funct. Mater.* **2014**, *24*, 117.
[19] Y. Wang, L. Wang, T. Yang, X. Li, X. Zang, M. Zhu, K. Wang, D. Wu, H. Zhu, *Adv. Funct. Mater.* **2014**, *24*, 4666.
[20] S. Zhu, Y. Gao, B. Hu, J. Li, J. Su, Z. Fan, J. Zhou, *Nanotechnology* **2013**, *24*, 5202.
[21] J. Zhong, Y. Zhang, Q. Zhong, Q. Hu, B. Hu, Z. L. Wang, J. Zhou, *ACS Nano* **2014**, *8*, 6273.
[22] J. Zhong, Q. Zhong, F. Fan, Y. Zhang, S. Wang, B. Hu, Z. L. Wang, J. Zhou, *Nano Energy* **2013**, *2*, 491.
[23] Q. Zhong, J. Zhong, B. Hu, Q. Hu, J. Zhou, Z. L. Wang, *Energy Environ. Sci.* **2013**, *6*, 1779.
[24] H. Gullapalli, V. S. M. Vemuru, A. Kumar, A. Botello-Mendez, R. Vajtai, M. Terrones, S. Nagarajaiah, P. M. Ajayan, *Small* **2010**, *6*, 1641.
[25] A. V. Shirinov, W. K. Schomburg, *Sens. Actuators A Phys.* **2008**, *142*, 48.
[26] J. Soman, C. B. O'Neal, *IEEE Sens. J.* **2011**, *11*, 78.